nanomaterials

MDPI

Article

Feasible Route for a Large Area Few-Layer MoS_2 with Magnetron Sputtering

Wei Zhong [1,†], Sunbin Deng [2,†], Kai Wang [2], Guijun Li [2], Guoyuan Li [1], Rongsheng Chen [1,2,*] and Hoi-Sing Kwok [2]

1 School of Electronic and Information Engineering, South China University of Technology, Guangzhou 510640, China; zwnice@163.com (W.Z.); phgyli@scut.edu.cn (G.L.)

2 State Key Laboratory on Advanced Displays and Optoelectronics Technologies, Department of Electronic and Computer Engineering, The Hong Kong University of Science and Technology, Hong Kong, China; sdengaa@connect.ust.hk (S.D.); kaiwjnu@163.com (K.W.); gliad@connect.ust.hk (G.L.); eekwok@ust.hk (H.-S.K.)

* Correspondence: rschen@connect.ust.hk; Tel.: +86-20-8711-1435

† These authors have contributed equally to this work.

Received: 20 June 2018; Accepted: 30 July 2018; Published: 3 August 2018

Abstract: In this article, we report continuous and large-area molybdenum disulfide (MoS_2) growth on a SiO_2/Si substrate by radio frequency magnetron sputtering (RFMS) combined with sulfurization. The MoS_2 film was synthesized using a two-step method. In the first step, a thin MoS_2 film was deposited by radio frequency (RF) magnetron sputtering at 400 °C with different sputtering powers. Following, the as-sputtered MoS_2 film was further subjected to the sulfurization process at 600 °C for 60 min. Sputtering combined with sulfurization is a viable route for large-area few-layer MoS_2 by controlling the radio-frequency magnetron sputtering power. A relatively simple growth strategy is demonstrated here that simultaneously enhances thin film quality physically and chemically. Few-layers of MoS_2 are established using Raman spectroscopy, X-ray diffractometer, high-resolution field emission transmission electron microscope, and X-ray photoelectron spectroscopy measurements. Spectroscopic and microscopic results reveal that these MoS_2 layers are of low disorder and well crystallized. Moreover, high quality few-layered MoS_2 on a large-area can be achieved by controlling the radio-frequency magnetron sputtering power.

Keywords: few-layer MoS_2; magnetron sputtering; magnetron sputtering power; raman spectroscopy; disorder

1. Introduction

The emergence of monolayer graphene [1,2] and transition metal dichalcogenides (TMDs) [3,4] has inspired a series of high-profile discoveries in the electronic and optoelectronic fields [5–7], and has initiated potentially new areas [8,9]. Thus, two-dimensional (2D) materials have recently been intensively studied. In the context of 2D TMDs, molybdenum disulfide (MoS_2) is one of the attractive embodiments due to its stable form in few- and single-layers [10,11] as well as its desirable electrical and optical properties [12]. Few- and single-layer MoS_2 is firstly obtained via top-down mechanical stripping techniques [13], which are commonly used for graphene exfoliation. Although this method of exfoliation and dip coating [14–17] has its own the advantages to achieve high-quality 2D materials, none of these are proper solutions for radical large-scale commercial manufacturing, where the mass-producible growth of large-area, continuous, and high-quality 2D MoS_2 thin films on dielectrics is a pre-requisite. From this point of view, the bottom-up strategies for thin film growth, including chemical vapor deposition (CVD) and physical vapor deposition (PVD), are better choices when

compared with the top-down methods mentioned above. CVD methods have already been successfully demonstrated [18–20], but the control of thin film thickness, purity and uniformity on a large scale needs to be further enhanced [21]. On the other hand, PVD methods, especially magnetron sputtering, have been broadly employed in large-scale commercial manufacturing at low cost and with easy control. However, the exploration of 2D MoS_2 thin film growth using magnetron sputtering technology is quite insufficient [21]. In recent years, there have been few attempts at sputtering techniques for the growth of MOS_2 thin films. Muratore et al. [22], Kaindl et al. [23], and Samassekou et al. [24] reported the synthesis of continuous few-layer MoS_2 by sputtering method using a MoS_2 target, and the sputtered MoS_2 films was annealed in an argon atmosphere. Tao et al. [21] and Santoni et al. [25] reported MoS_2 film using Mo target sputtered in vaporized sulfur ambient. However, the reported films either are relatively thick or have poor crystal quality and optical properties [21–25]. The main obstacles for large-area sputtered high quality MoS_2 films are possibly located in the difficulty of disorder control during thin film deposition, and the lack of metrics to evaluate the deposited thin films.

Studies over the past decade have shown that Raman spectroscopy has historically played an important role in the structural characterization of graphitic materials [26–28] and has also become a powerful tool to understand the effects of process parameters on the production of high quality graphene by monitoring changes in disordered peaks [28–32]. Recently, Raman spectroscopy has also been used to study the effects of disorder on the MoS_2 [33]. On the other hand, since many scholars have previously investigated the crystallinity of MoS_2 thin film by high-temperature vulcanization or deposition on different substrates [21,34,35], few studies have investigated the effect of sputtering power on the MoS_2 thin film. Therefore, in this work, we use a Raman spectroscopy approach to describe the quality and to study the effect of RF power on the deposition of the large-scale few-layer MoS_2 films. We also investigated the crystalline structure of the films through an X-ray diffractometer (XRD) and a high-resolution field emission transmission electron microscope (HRTEM). The binding energies of Mo in the MoS_2 film grown by radio frequency magnetron sputtering (RFMS) were further analyzed by X-ray photoelectron spectroscopy (XPS). For precise detection, the surface 5-nm-thick thin films were etched using Ar ions before XPS characterization.

2. Materials and Methods

The large-scale few layer MoS_2 thin films were deposited using the RFMS technique. Firstly, both silicon substrates coated with thermally grown SiO_2 and glass substrates (Eagle 2000, Corning) were ultrasonically cleaned in acetone and then isopropanol (IPA). After being rinsed in deionized (DI) water and dried, the substrates were loaded into the chamber of an RFMS system (AJA International Inc., Scituate, MA, USA) and heated to 400 °C. The distance between the substrate and the MoS_2 target (99.99%, 2 Inc., Plasmaterials Inc., Livermore, CA, USA) was 10 cm. In order to suppress the influence of oxygen and moisture on the deposited thin films, the base pressure of the chamber should be pumped down as low as possible. In this work, the value was 2.67×10^{-5} Pa. During deposition, Ar gas (99.999%) was allowed to flow into the chamber with a stable flow rate of 20 sccm, and the working pressure of the chamber was maintained at 3×10^{-3} Torr. The RF sputtering power applied to the MoS_2 target was varied from 10 W to 150 W in order to investigate the relationship between the large-scale few layer MoS_2 growth and RF power. The deposition time was dependent on the required thickness of the thin films and the thickness of the film is maintained at 15 nm, the thickness of the thin films is confirmed by HRTEM (High-Resolution Transmission Electron Microscopy). When the RFMS process was completed, the heater and the Ar gas pipeline were switched off, and the substrates were cooled down to room temperature naturally. After loading out of the chamber, the SiO_2/Si substrates and glass substrates with as-deposited MoS_2 thin film were immediately subjected to post-annealing in a sulfurization atmosphere for 60 min at 600 °C to enhance thin film quality physically and chemically (Figure 1).

In order to identify the layered structure and obtain the disorder information, the deposited MoS_2 thin films were analyzed using Raman spectroscopy (Renishaw invia RE04, 514 nm Ar laser with a 1 μm

spot size, Renishaw plc, Gloucestershire, United Kingdom). For the crystalline phase characterizations of the thin films, an X-ray diffractometer (XRD, Empyrean, PANalytical, Almelo, The Netherlands) with Cu Kα radiation was used. It was operated in thin-film mode, and the angle between the X-ray and the thin film surface was fixed at 0.5 degrees. Furthermore, a high-resolution transmission electron microscopy (HRTEM, JEM-2010HR, JEOL, Tokyo, Japan) was applied to identify the number of layers and atomic structure of the MoS_2 film. To analyze the material composition of the deposited thin films as well as the chemical environment of the atoms in the thin films, X-ray photoelectron spectroscopy (XPS) measurement was conducted on the Physical Electronics 5600 multi-technique system (Physical Electronics Inc., Chanhassen, MN, USA).

3. Results and Discussion

Figure 1 shows an image of MoS_2 thin layer grown on glass substrates with different deposition time (15 s, 30 s, and 45 s). The deposited MoS_2 layer was light gray, and after annealing under a sulfur atmosphere, the MoS_2 layer was pale yellow and was found to have specular reflection of ambient light. This result is consistent with previous reports [21]. The size of the synthesized films is limited by the dimensions of our sample heating holder.

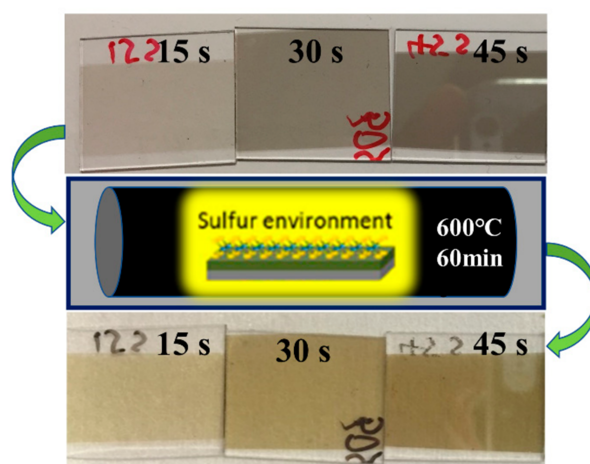

Figure 1. This post-deposition annealing treatment was performed to further enhance crystalline quality in as-sputtered MoS_2 on glass substrates under sulfur environment.

Figure 2 shows the Raman spectra of the MoS_2 thin films on SiO_2/Si substrates deposited under different RF powers of 10 W, 80 W, 120 W and 150 W, respectively. From Figure 2, it can be seen that all of the thin films exhibit two specific Raman characteristic peaks of MoS_2, namely the in-plane (E^1_{2g}) peak at ~381 cm^{-1} and the out-of-plane (A_{1g}) peak at ~405 cm^{-1}. Their peak positions herein are quite consistent with the results in other reports [24,36,37] , which the E^1_{2g} and A_{1g} mode peaks appear at ~381.5 cm^{-1} and ~404.8 cm^{-1}. Besides this, a relatively small LA(M) peak (a defect peak generated by LA phonons at the M point in the Brillouin zone) is also observed at ~227 cm^{-1}. Theoretically, the E^1_{2g} mode corresponds to the S and Mo atoms oscillating in antiphase parallel to the crystal plane, while the A_{1g} mode corresponds to the S atoms oscillating in antiphase out-of-plane, as shown in the insets of Figure 2 [29,38]. In addition to the absolute positions of these two peaks, the frequency difference (Δk) between the A_{1g} peak and the E^1_{2g} peak is a good indicator of the layer number in MoS_2 thin films. In this work, Δk is around 24 cm^{-1}, which is larger than that in monolayer MoS_2 thin films (~18–19 cm^{-1}) [19,33,39], but smaller than the typical value in bulk MoS_2 (~26 cm^{-1}) [37,38]. This indicates the existence of few-layer MoS_2 [36]. Table 1 lists the peak positions corresponding to the E^1_{2g} and A_{1g} mode as well as the Δk values for all samples under various RF sputtering powers in this work. With the continuous increase of RF power from 10 W to 150 W, the Δk values remain in the

vicinity of 24 cm^{-1}. This means that all of the thin films under different RF powers are MoS_2 with a few layers [36,37]. Another indicator of film quality is the full width at half maxima (FWHM) of the observed vibration modes. FMHM values for the sputtered FL-MoS_2 film with different RF powers is compared in Table 1. In general, higher FMHM values mean more disorder [24,25]. From the Table 1, it can be seen that the MoS_2 films with RF powers of 120 W has the lowest FMHM values, meaning it has the least disorder. It also can be seen that the A_{1g} peak and the E^1_{2g} peak all have a blue shift as the RF powers increased from 10 W to 120 W and a red shift as the RF powers increased from 120 W to 150 W. The red shift is attributed to the high RF power, resulting in an increase in the residual-stress of the film [40].While the blue shift is attributed to O_2-doping of MoS_2, which will be shown on the XPS result [41].

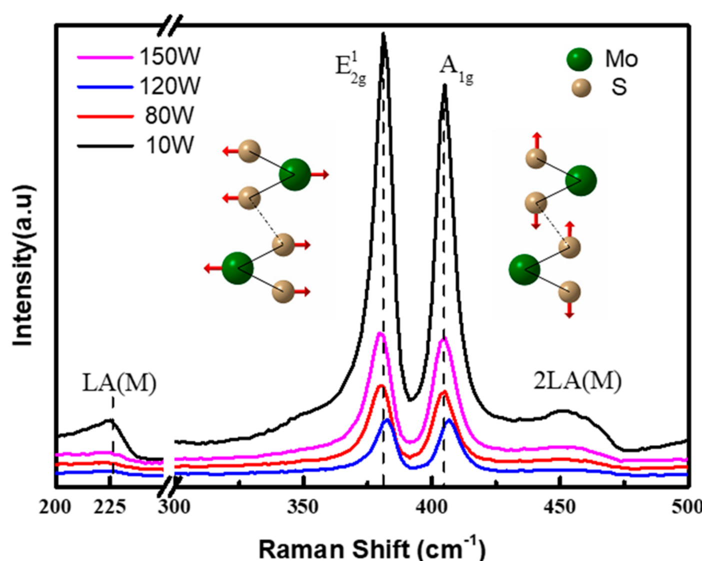

Figure 2. Raman spectra of the MoS_2 thin films deposited on SiO_2/Si substrates under different radio frequency (RF) powers. The insets illustrate the oscillating mode of the E^1_{2g} and A_{1g} peak.

According to Raman fundamental selection rules, only phonons with wave vector q ≅ 0 are Raman active around the center of the Brillouin zone. However, this rule will be broken by defects, which cause the appearance of peaks away from the zone center [33,42]. Monitoring the evolution of disorder-related sub-peaks in the Raman spectrum enables us to understand the effects of process parameters and has allowed great strides to be made in the CVD preparation of high quality graphene [29,43,44]. Similarly, in Figure 2, apart from two major peaks with regard to the basic E^1_{2g} and A_{1g} vibration modes, several sub-peaks related to the defects can also be observed. Among them, the sub-peak at 227 cm^{-1} is the most intense, which is attributed to the longitudinal phonon branch at the point M (LA (M)) of the Brillouin region [33,45]. Therefore, this sub-peak is able to form a very clear marker for disorder in the system, especially for the few- and single-layer MoS_2. The intensity ratio of the LA(M) sub-peak to A_{1g} peak is plotted as a function of RF power in Figure 3. It can be clearly observed that the intensity ratio reaches a minimum when the RF power climbs to 120 W, indicating the improvement of thin film quality [46]. In general, higher RF power could assist with the formation of crystalline films with lower disorder (namely, lower LA(M)/ A_{1g} intensity ratio), but excessively high RF power is not welcomed. For instance, the LA(M)/A_{1g} intensity ratio rises when the RF power increases from 120 W to 150 W. It reveals the increase of disorder in the deposited MoS_2 thin films. A possible explanation for this phenomenon could be the increased defect generation caused by ion bombardment under over-high RF power.

Table 1. The E^1_{2g}- and A_{1g}-related Raman peak information of MoS_2 thin films deposited using radio frequency magnetron sputtering (RFMS) under various RF powers.

RF Power (W)	A_{1g} (cm^{-1})	E^1_{2g} (cm^{-1})	Δk (A_{1g}-E^1_{2g}) (cm^{-1})	Full Width at Half-Maximum (cm^{-1})		LA(M) to A_{1g} Peak Intensity Ration
				A_{1g}	E^1_{2g}	
10	405.2 ± 0.1	381.2 ± 0.1	24.0 ± 0.02	10.64 ± 0.46	10.87 ± 0.56	0.219 ± 0.010
80	405.4 ± 0.4	381.4 ± 0.4	24.0 ± 0.01	10.17 ± 0.34	10.31 ± 0.21	0.195 ± 0.004
120	407.0 ± 0.1	383.0 ± 0.1	24.0 ± 0.02	9.55 ± 0.02	9.57 ± 0.20	0.180 ± 0.003
150	403.7 ± 0.4	379.7 ± 0.4	24.0 ± 0.02	10.49 ± 0.13	10.56 ± 0.02	0.204 ± 0.006

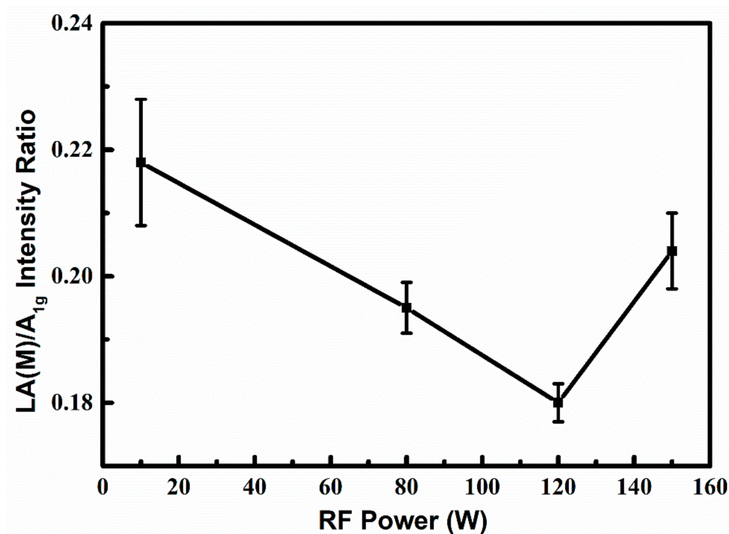

Figure 3. LA(M) to A_{1g} peak intensity ratio of the MoS_2 films with different RF powers deposited on SiO_2/Si substrates.

The crystalline information of the samples was characterized using XRD. The X-ray diffraction patterns of MoS_2 thin films on SiO_2/Si substrates under different RF powers are shown in Figure 4. The MoS_2 thin films deposited under different RF powers all exhibit three obvious diffraction peaks, which are located at 14.0°, 21.6°, and 51.5° respectively. The two weak diffraction peaks at 21.6° and 51.5° correspond to the SiO_2 (JCPDS: 27-0605) (111) and (400) planes, respectively. The strong diffraction peak at 14.0° is an indicator of the MoS_2 (JCPDS: 37-1492) (002) plane. For the MoS_2 thin films deposited under an RF power of 10 W, the broad and weak diffraction peak at 14.0° indicates the amorphous structure of the film. However, when the RF power increases to 80 W, 120 W and then 150 W, all of the MoS_2 thin films exhibit a strong and narrow diffraction peak at 14.0°, which indicate the well crystallization of MoS_2 thin films. Since the (002) plane is parallel to the surface of the substrates, the deposited MoS_2 thin films using the RFMS technique under an RF power of 80 W, 120 W and 150 W could grow along the c-axis. Meanwhile, the exclusive diffraction peak also suggests the thin films are highly oriented. These properties are quite helpful for the formation of stacked microstructures in MoS_2 thin films. Besides this, it should be noted that the intensity of the (002) peak for MoS_2 thin films under an RF power of 150 W is lower compared to the other two samples. This is possibly related to the degradation of crystalline quality under such high RF powers [47]. At the same time, we also noticed that under the RF power of 150 W, the sample showed a weak diffraction peak at 28.4°, which corresponds to the Si (JCPDS: 27-1402) (100) plane.

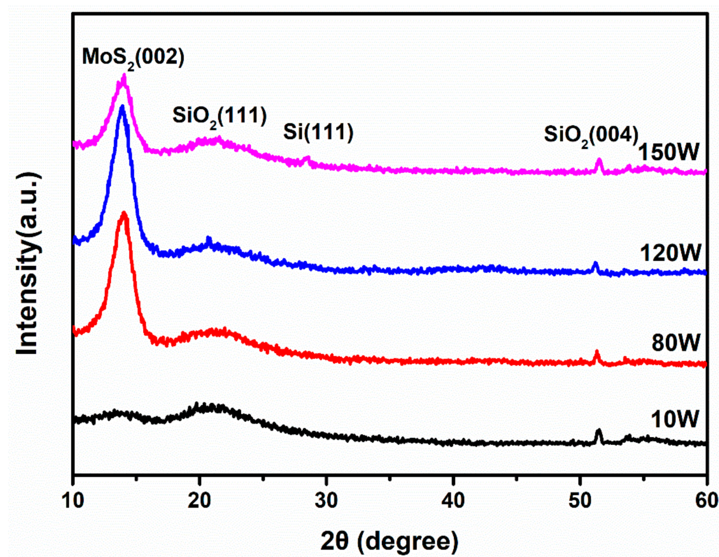

Figure 4. X-ray diffraction patterns of the MoS_2 thin films on SiO_2/Si substrates under different RF sputtering powers.

To further elucidate the crystalline structure, the MoS_2 thin film deposited by 120 W RF power was transferred onto a lacey copper grid for HRTEM characterizations. Figure 5a presents its cross-sectional HRTEM image, it can be seen that there are about 20 layers of the MoS_2 thin films on the SiO_2/Si substrate, and the interlayer spacing (0.68 nm) of the MoS_2 thin films is consistent with the previous results [21]. Moreover, it is also verified that the deposited MoS_2 thin films are stacked a few layers in parallel, which is in agreement with the results extracted from the Raman spectra above. As far as the typical high resolution TEM image in Figure 5b is concerned, the first-order diffraction spots of the FFT image (inset of Figure 5b) on a selected area are shown according to a regular hexagonal symmetry, thus indicating the presence of the MoS_2 thin film made of single crystal domains (without Moireé patterns). Moreover, HRTEM images of the selected area in Figure 5b after FFT filtering are shown in Figure 5c. The IFFT-filtered image (Figure 5c) shows a regular honeycomb pattern due to the atomic arrangements of the Mo and S atoms. In Figure 5d, the calculated profile along the selected direction in Figure 5c is drawn, which reveals the (004) plane of MoS_2 with a lattice spacing of 0.31 nm that is observed in Figure 5c. Figure 5e is the magnified image of the square-surrounded region in Figure 5c. The periodic atom arrangement for Mo confirms that the MoS_2 thin films deposited under an RF power of 120 W own a crystalline structure. This is also consistent with the XRD results in Figure 4.

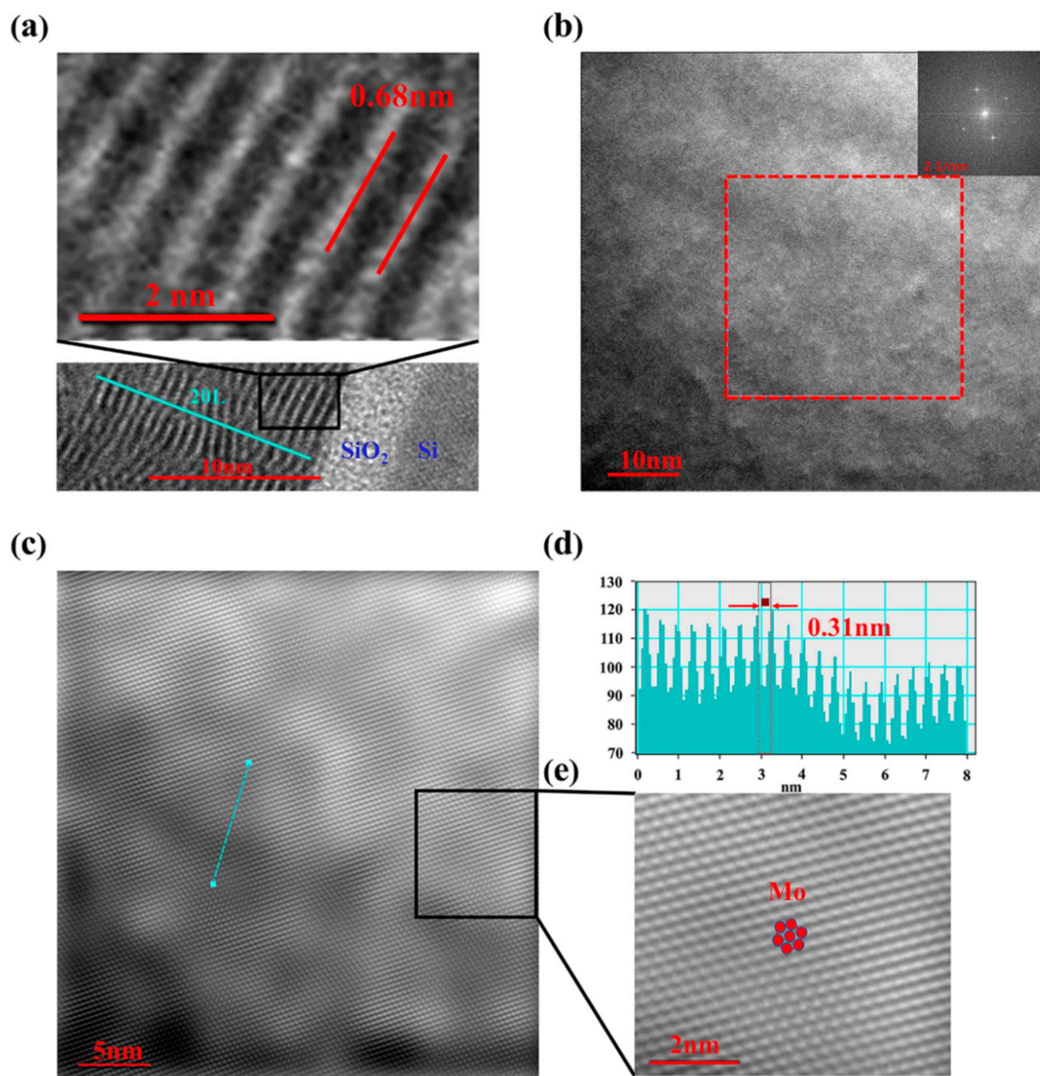

Figure 5. (**a**) Cross-sectional high-resolution field emission transmission electron microscope (HRTEM) image of samples deposited under an RF power of 120 W. (**b**) High resolution TEM image of the MoS_2 film deposited by 120 W RF power transferred onto a lacey carbon grid. The inset shows the fast Fourier transformation (FFT) image corresponding to the TEM image selected area of a portion of (**b**), showing the hexagonal symmetry of the MoS_2 structure. (**c**) Inverse FFT images corresponding to the TEM image selected area of a portion of (**b**). (**d**) Atomic spacing along the selected direction of the basal plane. (**e**) Zoom-in image of the area highlighted in (**c**). The hexagonal structure formed by Mo atoms is indicated.

XPS was used to analyze the chemical environment of Mo in the MoS_2 thin films, and to detect any impurity (particularly oxygen) involvement during preparation. The high-resolution XPS spectra of the Mo 3d and S 2s region are shown in Figure 6. Since the peaks of Mo 3d and S 2s are too close to distinguish, in order to obtain the chemical environment information of the Mo species, both the S 2s and Mo 3d spectra are taken into account. Moreover, since the main Mo doublet peak signals of the thin films under an RF power of 10 W are so weak that they reach noise level, the analysis in terms of such samples is not reliable. Hence, only the data with an RF power of 80 W, 120 W and 150 W have been fitted by a 20% Lorentzian–Gaussian ration fit and the according results together with the Shirley background are presented in Figure 6b–d. According to [35], the two peaks at 229.1 eV and 232.2 eV for the MoS_2 thin film are attributed to the doublet Mo $3d_{5/2}$ and Mo $3d_{3/2}$ orbitals, respectively. Meanwhile, the fitting shows that there is a second characteristic at the lower binding

energy. For species originating from lower binding energy (BE) Mo3d peaks, the lower BE Mo species is Mo still associated with the Mo-S lattice, or it reflects a single amorphous MoS_x phase, where Mo has a different number of nearest neighbor S atoms [48,49]. According to [25], the lower BE Mo species can be assigned to zero-valent Mo (Mo(0)) occurring in small aggregates dispersed in a MoS_2 matrix. From the principle of sputter coating, we can know that the presence of Mo(0) cannot be avoided, and the purpose of annealing under a sulfur atmosphere is to convert Mo(0) to Mo(IV), which can reduce disorder and defect formation. However, when the film is etched by an ion beam, there is also a chemical shift of its binding energy toward smaller values [25,35]. Therefore, compared to XPS characterization, the advantages of strong non-destructive characterization of Raman spectra are even more pronounced. For accurate detection, 5-nano-thin-thick-surface films should be etched with Ar ions prior to XPS characterization. However, this will lead to sample destruction and will have a certain impact on the test results. Although this changed the chemical state of the Mo atom, all the samples were processed in the same way, and the overall trend of its variation with sputtering power did not change. The relative ratio of Mo species calculated from the deconvolved Mo 3d spectrum results is shown in Figure 7. The Mo(IV) fraction is defined as the area under the Mo(IV) peak divided by the total Mo peak area. It can clearly be seen that the Mo (IV) fraction reaches a maximum when the RF power is increased to 120 W, indicating the improvement of thin film quality. In addition, smaller peaks at 230.2 eV and 233.3 eV are assigned to Mo^{5+} [50], indicating the presence of chemisorbed oxygen at sulfur vacancies [51,52] or sub-stoichiometric oxides MoO_x [53]. The origin of MoO_x is probably due to the sulfurization process. We believe that MoO_x has probably formed during the deposition and/or during the sulfurization process at 600 °C by reaction with the oxygen diffused from the SiO_2/Si substrate. As shown in Figure 7, the Mo (V) fraction is around 0.1, 0.094 and 0.102 for an RF power of 80 W, 120 W, and 150 W, respectively. For different RF powers, the Mo(V) fraction is basically the same, indicating that the power change has no effect on the Mo(V) fraction.

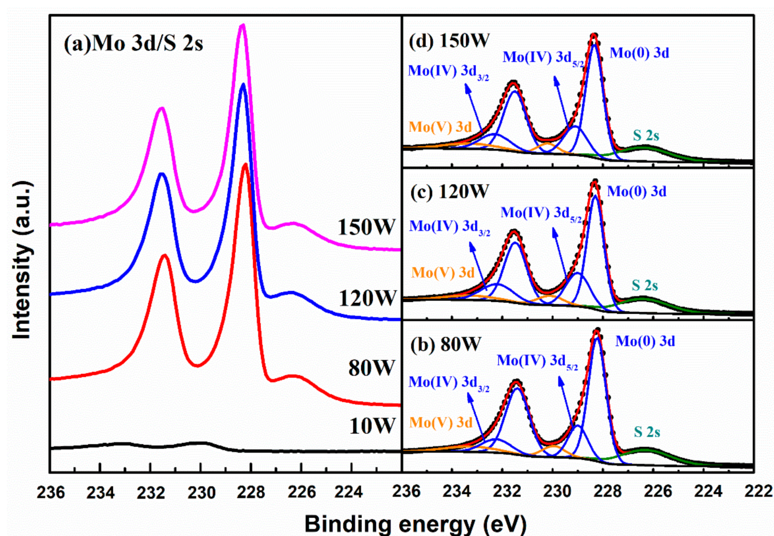

Figure 6. High-resolution X-ray photoelectron spectroscopy (XPS) spectra of (**a**) Mo 3d/S 2s, and (**b**), (**c**), and (**d**) Mo3d core-level spectra for an RF power of 80 W, 120 W, and 150 W, respectively. The background is shown with a black line at the bottom. The black dots represent the raw data. The red line is the total least-squares fit. The orange lines indicate the Mo(V) 3d components. The blue lines are the Mo3d components linked to Mo (0) and Mo (IV), the Mo (0) are the lower BE doublet. The olive lines are the S2s components. (See text for more explanation).

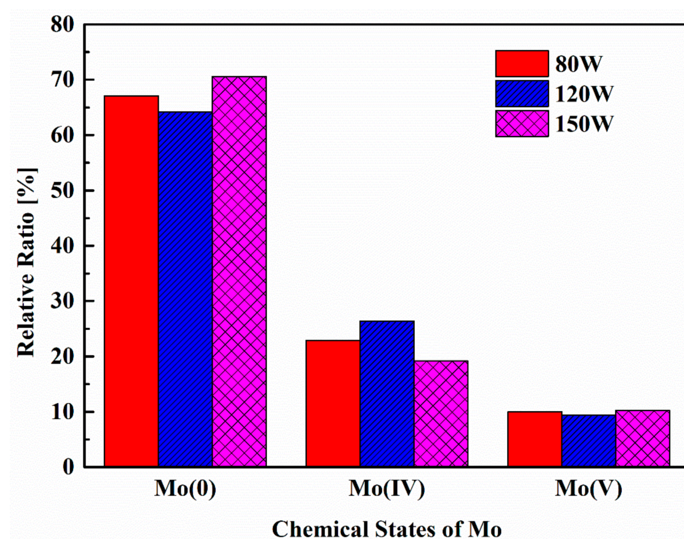

Figure 7. Relative ratio of Mo species with various chemical states at different RF powers.

4. Conclusions

Few-layer MoS_2 thin film deposition on large-area thermally oxidized silicon substrates was demonstrated using the RFMS technique. Raman analysis verified the achievement of few-layer MoS_2 thin films. Meanwhile, it was proposed that the disorder inside the thin films could be monitored using Raman spectra, and controlled by adjusting the RF sputtering power. Furthermore, the XRD spectra and cross-sectional TEM images confirmed the high quality of few-layer MoS_2 thin films, implying that RFMS was suitable for layered MoS_2 growth. Additionally, the XPS characterizations on RFMS grown few-layer MoS_2 thin films revealed the RF power has a great effect on the binding energies of Mo atoms. Our work illustrates that sputtering combined with sulfurization is a viable route for the high quality of large-area few-layer MoS_2 by controlling the radio-frequency magnetron sputtering power.

Author Contributions: S.D. and K.W. conceived and designed the experiments; S.D. and K.W. performed the experiments; W.Z. and R.C. analyzed the data; S.D., K.W., W.Z. and G.L. (Guijun Li). contributed materials/analysis tools; W.Z., S.D. and R.C. wrote the paper; G.L. (Guoyuan Li) and H.-S.K. provided advice about the content and the structure of this work.

Funding: This research was funded by the National Natural Science Foundation of China under Grant 61604057, in part by the Partner State Key Laboratory on Advanced Displays and Optoelectronics Technologies under Grant ITC-PSKL12EG02, in part by the Science and Technology Program of Guangdong Province under Grant 2017A010101010, and in part by the Science and Technology Program of Guangdong Province under Grant No. 201807010098.

Conflicts of Interest: The authors declare no conflict of interest.

References

1. Guinea, F.; Peres, N.M.R.; Novoselov, K.S.; Geim, A.K.; Castro Neto, A.H. The electronic properties of graphene. *Rev. Mod. Phys.* **2009**, *81*, 109–162.
2. Geim, A.K.; Novoselov, K.S. The rise of graphene. *Nat. Mater.* **2007**, *6*, 183–191. [CrossRef] [PubMed]
3. Miró, P.; Audiffred, M.; Heine, T. An atlas of two-dimensional materials. *Chem. Soc. Rev.* **2014**, *43*, 6537–6554. [CrossRef] [PubMed]
4. Kuc, A. Low-dimensional transition-metal dichalcogenides. In *Chemical Modelling*; Royal Society of Chemistry: London, UK, 2014; Volume 11, pp. 1–29.
5. Fiori, G.; Bonaccorso, F.; Iannaccone, G.; Palacios, T.; Neumaier, D.; Seabaugh, A.; Banerjee, S.K.; Colombo, L. Electronics based on two-dimensional materials. *Nat. Nanotechnol.* **2014**, *9*, 768–779. [CrossRef] [PubMed]
6. Wang, Q.H.; Kalantar-Zadeh, K.; Kis, A.; Coleman, J.N.; Strano, M.S. Electronics and optoelectronics of two-dimensional transition metal dichalcogenides. *Nat. Nanotechnol.* **2012**, *7*, 699–712. [CrossRef] [PubMed]

7. Kang, K.; Xie, S.; Huang, L.; Han, Y.; Huang, P.Y.; Mak, K.F.; Kim, C.J.; Muller, D.; Park, J. High-mobility three-atom-thick semiconducting films with wafer-scale homogeneity. *Nature* **2015**, *520*, 656–660. [CrossRef] [PubMed]
8. Zeng, H.; Dai, J.; Yao, W.; Xiao, D.; Cui, X. Valley polarization in MoS_2 monolayers by optical pumping. *Nat. Nanotechnol.* **2012**, *7*, 490–493. [CrossRef] [PubMed]
9. Mak, K.F.; He, K.; Shan, J.; Heinz, T.F. Control of valley polarization in monolayer MoS_2 by optical helicity. *Nat. Nanotechnol.* **2012**, *7*, 494–498. [CrossRef] [PubMed]
10. Novoselov, K.S.; Jiang, D.; Schedin, F.; Booth, T.J.; Khotkevich, V.V.; Morozov, S.V.; Geim, A.K. Two-dimensional atomic crystals. *Proc. Natl. Acad. Sci. USA* **2005**, *102*, 10451–10453. [CrossRef] [PubMed]
11. Mak, K.F.; Lee, C.; Hone, J.; Shan, J.; Heinz, T.F. Atomically thin MoS_2: A new direct-gap semiconductor. *Phys. Rev. Lett.* **2010**, *105*, 136805. [CrossRef] [PubMed]
12. Lin, Z.; Mccreary, A.; Briggs, N.; Subramanian, S.; Zhang, K.; Sun, Y.; Li, X.; Borys, N.J.; Yuan, H.; Fullerton-Shirey, S.K.; et al. 2D materials advances: From large scale synthesis and controlled heterostructures to improved characterization techniques, defects and applications. *2D Mater.* **2016**, *3*, 042001. [CrossRef]
13. Radisavljevic, B.; Radenovic, A.; Brivio, J.; Giacometti, V.; Kis, A. Single-layer MoS_2 transistors. *Nat. Nanotechnol.* **2011**, *6*, 147–150. [CrossRef] [PubMed]
14. Li, Y.; Xu, C.Y.; Hu, P.A.; Zhen, L. Carrier Control of MoS_2 Nanoflakes by Functional Self-Assembled Monolayers. *ACS Nano* **2013**, *7*, 7795–7804. [CrossRef] [PubMed]
15. Sundaram, R.S.; Engel, M.; Lombardo, A.; Krupke, R.; Ferrari, A.C.; Avouris, P.; Steiner, M. Electroluminescence in single layer MoS_2. *Nano Lett.* **2013**, *13*, 1416–1421. [CrossRef] [PubMed]
16. Das, S.; Chen, H.Y.; Penumatcha, A.V.; Appenzeller, J. High performance multilayer MoS_2 transistors with scandium contacts. *Nano Lett.* **2013**, *13*, 100–105. [CrossRef] [PubMed]
17. Sik Hwang, W.; Remskar, M.; Yan, R.; Kosel, T.; Kyung Park, J.; Cho, B.J.; Haensch, W.; Grace Xing, H.; Seabaugh, A.; Jena, D. Comparative study of chemically synthesized and exfoliated multilayer MoS_2 field-effect transistors. *Appl. Phys. Lett.* **2013**, *102*, 043116. [CrossRef]
18. Elibol, K.; Susi, T.; M, O.B.; Bayer, B.C.; Pennycook, T.J.; Mcevoy, N.; Duesberg, G.S.; Meyer, J.C.; Kotakoski, J. Grain boundary-mediated nanopores in molybdenum disulfide grown by chemical vapor deposition. *Nanoscale* **2016**, *9*, 1591–1598. [CrossRef] [PubMed]
19. Lee, Y.H.; Zhang, X.Q.; Zhang, W.; Chang, M.T.; Lin, C.T.; Chang, K.D.; Yu, Y.C.; Wang, J.T.; Chang, C.S.; Li, L.J.; et al. Synthesis of large-area MoS_2 atomic layers with chemical vapor deposition. *Adv. Mater.* **2012**, *24*, 2320–2325. [CrossRef] [PubMed]
20. Zhan, Y.; Liu, Z.; Najmaei, S.; Ajayan, P.M.; Lou, J. Large Area Vapor Phase Growth and Characterization of MoS_2 Atomic Layers on SiO_2 Substrate. *Small* **2012**, *8*, 966–971. [CrossRef] [PubMed]
21. Tao, J.; Chai, J.; Lu, X.; Wong, L.M.; Wong, T.I.; Pan, J.; Xiong, Q.; Chi, D.; Wang, S. Growth of wafer-scale MoS_2 monolayer by magnetron sputtering. *Nanoscale* **2015**, *7*, 2497–2503. [CrossRef] [PubMed]
22. Muratore, C.; Hu, J.J.; Wang, B.; Haque, M.A. Continuous ultra-thin MoS_2 films grown by low-temperature physical vapor deposition. *Appl. Phys. Lett.* **2014**, *104*, 261604. [CrossRef]
23. Kaindl, R.; Bayer, B.C.; Resel, R.; Muller, T.; Skakalova, V.; Habler, G.; Abart, R.; Cherevan, A.S.; Eder, D.; Blatter, M.; et al. Growth, structure and stability of sputter-deposited MoS_2 thin films. *Beilstein J. Nanotechnol.* **2017**, *8*, 1115–1126. [CrossRef] [PubMed]
24. Samassekou, H.; Alkabsh, A.; Wasala, M.; Eaton, M.; Walber, A.; Walker, A.; Pitkanen, O.; Kordas, K.; Talapatra, S.; Jayasekera, T.; et al. Viable route towards large-area 2D MoS_2 using magnetron sputtering. *2D Mater.* **2017**, *4*, 021002. [CrossRef]
25. Santoni, A.; Rondino, F.; Malerba, C.; Valentini, M.; Mittiga, A. Electronic structure of Ar^+ ion-sputtered thin-film MoS_2: A XPS and IPES study. *Appl. Surf. Sci.* **2017**, *392*, 795–800. [CrossRef]
26. Pimenta, M.A.; Neves, B.R.A.; Medeiros-Ribeiro, G.; Enoki, T.; Kobayashi, Y.; Takai, K.; Fukui, K.; Dresselhaus, M.S.; Saito, R.; Jorio, A.; et al. Anisotropy of the Raman Spectra of Nanographite Ribbons. *Phys. Rev. Lett.* **2004**, *93*, 047403.
27. Wilhelm, H.; Lelaurain, M.; Mcrae, E.; Humbert, B. Raman spectroscopic studies on well-defined carbonaceous materials of strong two-dimensional character. *J. Appl. Phys.* **1998**, *84*, 6552–6558. [CrossRef]
28. Pimenta, M.A.; Dresselhaus, G.; Dresselhaus, M.S.; Cançado, L.G.; Jorio, A.; Saito, R. Studying disorder in graphite-based systems by Raman spectroscopy. *Phys. Chem. Chem. Phys.* **2007**, *9*, 1276–1290. [CrossRef] [PubMed]

29. Ferrari, A.C.; Basko, D.M. Raman spectroscopy as a versatile tool for studying the properties of graphene. *Nat. Nanotechnol.* **2013**, *8*, 235–246. [CrossRef] [PubMed]
30. Ferrari, A.C. Raman spectroscopy of graphene and graphite: Disorder, electron–phonon coupling, doping and nonadiabatic effects. *Solid State Commun.* **2007**, *143*, 47–57. [CrossRef]
31. Gupta, A.; Chen, G.; Joshi, P.; Tadigadapa, S.; Eklund, P.C. Raman Scattering from High-Frequency Phonons in Supported n-Graphene Layer Films. *Nano Lett.* **2006**, *6*, 2667–2673. [CrossRef] [PubMed]
32. Graf, D.; Molitor, F.; Ensslin, K.; Stampfer, C.; Jungen, A.; Hierold, C.; Wirtz, L. Spatially resolved Raman spectroscopy of single- and few-layer graphene. *Nano Lett.* **2007**, *7*, 238–242. [CrossRef] [PubMed]
33. Mignuzzi, S.; Pollard, A.J.; Bonini, N.; Brennan, B.; Gilmore, I.S.; Pimenta, M.A.; Richards, D.; Roy, D. Effect of disorder on Raman scattering of single-layer MoS_2. *Phys. Rev. B* **2015**, *91*, 195411. [CrossRef]
34. Liu, H.; Iskander, A.; Yakovlev, N.L.; Chi, D. Anomalous SiO_2 layer formed on crystalline MoS_2 films grown on Si by thermal vapor sulfurization of molybdenum at elevated temperatures. *Mater. Lett.* **2015**, *160*, 491–495. [CrossRef]
35. Hussain, S.; Singh, J.; Vikraman, D.; Singh, A.K.; Iqbal, M.Z.; Khan, M.F.; Kumar, P.; Choi, D.C.; Song, W.; An, K.S.; et al. Large-area, continuous and high electrical performances of bilayer to few layers MoS_2 fabricated by RF sputtering via post-deposition annealing method. *Sci. Rep.* **2016**, *6*, 30791. [CrossRef] [PubMed]
36. Hussain, S.; Shehzad, M.A.; Vikraman, D.; Khan, M.F.; Singh, J.; Choi, D.; Seo, Y.; Eom, J.; Lee, W.; Jung, J. Synthesis and characterization of large-area and continuous MoS_2 atomic layers by RF magnetron sputtering. *Nanoscale* **2016**, *8*, 4340–4347. [CrossRef] [PubMed]
37. Li, H.; Zhang, Q.; Yap, C.; Tay, B.; Edwin, T.; Olivier, A.; Baillargeat, D. From Bulk to Monolayer MoS_2: Evolution of Raman Scattering. *Adv. Funct. Mater.* **2012**, *22*, 1385–1390. [CrossRef]
38. Liu, Y.J.; Hao, L.Z.; Gao, W.; Liu, Y.M.; Li, G.X.; Xue, Q.Z.; Guo, W.Y.; Yu, L.Q.; Wu, Z.P.; Liu, X.H.; et al. Growth and humidity-dependent electrical properties of bulk-like MoS_2 thin films on Si. *RSC Adv.* **2015**, *5*, 74329–74335. [CrossRef]
39. Ganatra, R.; Zhang, Q. Few-Layer MoS_2: A Promising Layered Semiconductor. *ACS Nano* **2014**, *8*, 4074–4099. [CrossRef] [PubMed]
40. Taylor, C.A.; Wayne, M.F.; Chiu, W.K.S. Residual stress measurement in thin carbon films by Raman spectroscopy and nanoindentation. *Thin Solid Films* **2003**, *429*, 190–200. [CrossRef]
41. Piazza, A.; Giannazzo, F.; Buscarino, G.; Fisichella, G.; Magna, A.; Roccaforte, F.; Cannas, M.; Gelardi, F.M.; Agnello, S. In-situ monitoring by Raman spectroscopy of the thermal doping of graphene and MoS_2 in O_2-controlled atmosphere. *Beilstein J. Nanotech.* **2017**, *8*, 418–424. [CrossRef] [PubMed]
42. Richter, H.; Wang, Z.P.; Ley, L. The one phonon Raman spectrum in microcrystalline silicon. *Solid State Commun.* **1981**, *39*, 625–629. [CrossRef]
43. Ferrari, A.C.; Meyer, J.C.; Scardaci, V.; Casiraghi, C.; Lazzeri, M.; Mauri, F.; Piscanec, S.; Jiang, D.; Novoselov, K.S.; Roth, S. Raman spectrum of graphene and graphene layers. *Phys. Rev. Lett.* **2006**, *97*, 187401. [CrossRef] [PubMed]
44. Zhang, Y.; Zhang, L.; Zhou, C. Review of chemical vapor deposition of graphene and related applications. *Acc. Chem. Res.* **2013**, *46*, 2329–2339. [CrossRef] [PubMed]
45. Chakraborty, B.; Matte, H.; Sood, A.; Rao, C. Layer-dependent resonant Raman scattering of a few layer MoS_2. *J. Raman Spectrosc.* **2013**, *44*, 92–96. [CrossRef]
46. Mercado, E.; Goodyear, A.; Moffat, J.; Cooke, M.; Sundaram, R. A Raman metrology approach to quality control of 2D MoS_2 film fabrication. *J. Phys. D Appl. Phys.* **2017**, *50*, 184005. [CrossRef]
47. Laskar, M.R.; Nath, D.N.; Ma, L.; Lee, E.W. p-type doping of MoS_2 thin films using Nb. *Appl. Phys. Lett.* **2014**, *104*, 092104. [CrossRef]
48. Mcintyre, N.S.; Spevack, P.A.; Beamson, G.; Briggs, D. Effects of argon ion bombardment on basal plane and polycrystalline MoS_2. *Surf. Sci.* **1990**, *237*, L390–L397. [CrossRef]
49. Wagner, C.D.; Riggs, W.M.; Davis, L.E.; Moulder, J.F.; Muilenberg, G.E. *Handbook of X-ray Photoelectron Spectroscopy*; Perkin-Elmer Corporation, Physical Electronics Division Press: Eden Prairie, MN, USA, 1979; p. 190.
50. Al-Shihry, S.S.; Halawy, S.A. Unsupported MoO_3 Fe_2O_3 catalysts: Characterization and activity during 2-propanol decomposition. *J. Mol. Catal. A Chem.* **1996**, *113*, 479–487. [CrossRef]

51. Davis, S.M.; Carver, J.C. Oxygen chemisorption at defect sites in MoS_2 and ReS_2 basal plane surfaces. *Appl. Surf. Sci.* **1984**, *20*, 193–198. [CrossRef]
52. Ahn, C.; Lee, J.; Kim, H.U.; Bark, H.; Jeon, M.; Ryu, G.H.; Lee, Z.; Yeom, G.Y.; Kim, K.; Jung, J.; et al. Low-Temperature Synthesis of Large-Scale Molybdenum Disulfide Thin Films Directly on a Plastic Substrate Using Plasma-Enhanced Chemical Vapor Deposition. *Adv. Mater.* **2015**, *27*, 5223–5229. [CrossRef] [PubMed]
53. Choi, J.G.; Thompson, L.T. XPS study of as-prepared and reduced molybdenum oxides. *Appl. Surf. Sci.* **1996**, *93*, 143–149. [CrossRef]

© 2018 by the authors. Licensee MDPI, Basel, Switzerland. This article is an open access article distributed under the terms and conditions of the Creative Commons Attribution (CC BY) license (http://creativecommons.org/licenses/by/4.0/).